

Precision Spectroscopy of Kaonic Helium 3

$3d \rightarrow 2p$ X rays

June 15, 2015

M. Bazzi^a, D.A. Bennett^b, C. Berucci^c, D. Bosnar^d, C. Curceanu^a, W.B. Doriese^b,
J.W. Fowler^b, H. Fujioka^e, C. Guaraldo^a, F. Parnefjord Gustafsson^f, T. Hashimoto^g,
R.S. Hayano^{h*}, J.P. Hays-Wehle^b, G.C. Hilton^b, T. Hiraiwaⁱ, M. Iio^j, M. Iliescu^a,
S. Ishimoto^j, K. Itahashi^g, M. Iwasaki^{g,l}, Y. Ma^g, H. Noumiⁱ, G.C. O'Neil^b, H. Ohnishi^g,
S. Okada^{g†}, H. Outa^{g‡}, K. Piscicchia^a, C.D. Reintsema^b, Y. Sadaⁱ, F. Sakuma^g,
M. Sato^g, D.R. Schmidt^b, A. Scordo^a, M. Sekimoto^j, H. Shi^a, D. Sirghi^a, F. Sirghi^a,
K. Suzuki^c, D.S. Swetz^b, K. Tanida^k, H. Tatsuno^{b,i}, M. Tokuda^l, J. Uhlig^f,
J.N. Ullom^{b,m}, S. Yamadaⁿ, T. Yamazaki^h, and J. Zmeskal^c

^a Laboratori Nazionali di Frascati dell' INFN, Frascati, RM, I-00044, Italy

^b National Institute of Standards and Technology (NIST), Boulder, CO, 80303, USA

^c Stefan-Meyer-Institut für subatomare Physik, Vienna, A-1090, Austria

^d Department of Physics, University of Zagreb, Zagreb, HR-10000, Croatia

^e Department of Physics, Kyoto University, Kyoto, 606-8502, Japan

^f Department of Chemical Physics, Lund University, Lund, 221 00, Sweden

^g RIKEN Nishina Center, RIKEN, Wako, 351-0198, Japan

^h Department of Physics, The University of Tokyo, Tokyo, 113-0033, Japan

ⁱ Research Center for Nuclear Physics (RCNP), Osaka University, Osaka, 567-0047, Japan

^j High Energy Accelerator Research Organization (KEK), Tsukuba, 305-0801, Japan

^k Japan Atomic Energy Agency (JAEA), Tokai, 319-1184, Japan

^l Department of Physics, Tokyo Institute of Technology, Tokyo, 152-8551, Japan

^m Department of Physics, University of Colorado at Boulder, Boulder, CO, 80309-0390, USA

ⁿ Department of Physics, Tokyo Metropolitan University, Tokyo, 192-0397, Japan

*Spokesperson

†Co-spokesperson

‡Co-spokesperson

Executive Summary

We propose an experiment to measure the $2p$ -level strong interaction shifts of kaonic ${}^3\text{He}$ and ${}^4\text{He}$ atoms with a precision of 0.2 eV at J-PARC. The resulting sensitivity to small energy shift will provide valuable information regarding the isospin-dependent \bar{K} -nucleus interaction at zero energy, which will lead to a settlement of the long-standing deep-shallow problem of \bar{K} -nucleus potential strength.

This proposal supersedes the J-PARC E17 experiment proposal which was granted stage-2 approval. From the original proposal, we update the precision goal with an order of magnitude higher accuracy of determining the $2p$ level energy using a novel cryogenic x-ray detector instead of employing Silicon Drift Detectors (SDDs). The instrument, superconducting transition-edge-sensor (TES) microcalorimeter developed by NIST, has a FWHM energy resolution of 5 eV at 6 keV, whereas SDDs have typically 200 eV resolution. Direct measurements of the strong-interaction $2p$ -level widths become possible for the first time, if its magnitude exceeds ~ 2 eV. The unprecedented energy resolution allows as well a simultaneous measurement of kaonic- ${}^3\text{He}$ and kaonic- ${}^4\text{He}$ $3d \rightarrow 2p$ x rays whose energies are about 6.22 keV and 6.46 keV respectively, since a complete separation of the lines, 240 eV afar, is possible unlike SDDs. This will reduce the systematic errors of relative x-ray energies for both atoms. The feasibility of high-precision hadronic-atom x-ray spectroscopy with the TES spectrometer has been successfully demonstrated at PSI pion beamline.

The major parameters of this experiment are summarized below:

Reaction	: stopped $K^- + {}^3\text{He}$ or ${}^4\text{He} \rightarrow h\nu(\sim 6 \text{ keV}) + X$
Secondary beam	: 0.7 - 0.9 GeV/ c K^-
Beamline	: K1.8BR
Target	: mixed liquid ${}^3\text{He}$ and ${}^4\text{He}$ (diameter 6 cm, length 6 cm, $\sim 170 \text{ cm}^3$)
Detectors	: a 240-pixel array of TES microcalorimeters, and trigger counters
Beam time	: 3 days for K^- stop tune : 4 days for full commissioning : 100 kW·weeks for production run

Contents

1	Introduction	4
2	Experimental setup	7
2.1	TES microcalorimeter	7
2.2	Energy calibration source	9
2.3	Liquid helium target system	9
2.4	Trigger and data acquisition	10
3	Demonstration of TES operation at pion beamline	11
3.1	Experimental setup	11
3.2	Results of pionic-carbon 4-3 x-ray measurement	11
3.3	Effects due to charged-particle hit on TES system	14
4	Monte-Carlo study of K^- beamline at J-PARC	17
4.1	Yield estimation of the kaonic atom x-rays	17
4.2	Estimation of the charged-beam background	17
4.3	Estimation of the background in the final spectrum	19
5	Beam time request	21
6	Time schedule and cost estimation	22

1 Introduction

Kaonic atoms provide a unique laboratory to study the strong interaction between the kaon and atomic nucleus at the low-energy limit. Effects of the strong interaction appear in the most tightly bound energy level being the most perturbed by the strong force as a shift from that given only by the electromagnetic interaction, and a broadening due to absorption of the kaon by the nucleus. The shift and width can be experimentally extracted by performing characteristic x-ray-emission spectroscopy of the kaonic-atom x rays feeding the low-lying state.

Understanding of low-energy $\bar{K}N$ interaction has been substantially deepened by the most recent kaonic-hydrogen atom measurement [1] and its theoretical studies (e.g., [2]). However, the depth of \bar{K} -nucleus potential remains still unknown because of insufficient kaonic-atom data for $Z \geq 2$, which is tied closely to the puzzling situation on experimental and theoretical studies of kaonic nuclei.

There has been a conflict in the potential depth within two major theoretical approaches, so-called phenomenological model (e.g., [3]) and chiral unitary model (e.g., [4]), despite of the fact those theories reproduce the existing kaonic-atom data for $Z \geq 3$ [5,6]. The former is typically 180 MeV deep, whereas the latter is less than 50 MeV deep. Apart from kaonic-atom experiments, a lot of experimental search for the deeply-bound nuclear K^- states have been performed in a past decade. However, only a small amount of information is available [7–9], which is not sufficient to discriminate between a variety of conflicting interpretations. This is one of the greatest concerns in the recent strangeness nuclear physics.

Over 30 years ago, it was pointed out that a strong-interaction shift and width of $2p$ level in kaonic-helium atom (K^- -He) may appear near the resonance between atomic and nuclear poles and thus was expressed as a function of the potential depth [10]. For the two helium isotopes, K^- - ^4He and K^- - ^3He , the isoscalar and isovector strengths of the low-energy K^- -nucleus interaction result in the different shifts and widths for each atoms [11]. This clearly indicates that the precise measurement of $2p$ -level shift and width both for K^- - ^4He and K^- - ^3He atoms could yield valuable information concerning \bar{K} -nucleus potential at zero energy leading to a settlement of the long-standing deep-shallow problem in different models.

This situation motivated us to measure the strong-interaction shift of $3d \rightarrow 2p$ transition x rays of kaonic helium 4 atoms (~ 6.5 keV) in KEK-PS E570 [16], and to propose an experiment to measure the kaonic helium 3 x rays as stated in the J-PARC E17 original proposal [12] whose executive summary is attached in Appendix. After the stage-2 approval, E17 has been ready to run since January 2010 [13]; meanwhile SIDDHARTA collaboration at DAΦNE e^+e^- collider observed kaonic- ^3He $3d \rightarrow 2p$ x rays for the first time [14].

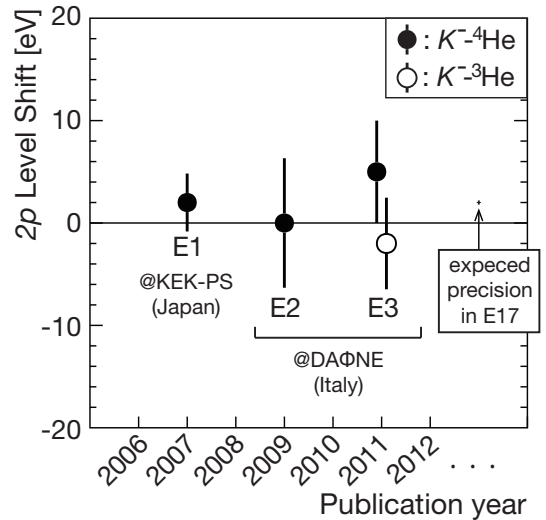


Figure 1: The $2p$ -level shift of kaonic ^3He and ^4He atoms obtained from the recent experiments at KEK-PS (E1 [16]) and DAΦNE (E2 [15], E3 [14]).

Figure 1 summarizes the recent measurements of the strong-interaction $2p$ -level shift of kaonic ${}^3\text{He}$ and ${}^4\text{He}$ atoms. Those experiments employed SDDs whose FWHM energy resolutions are typically ~ 200 eV at 6 keV [14–16]; thus resulting sensitivity to detect finite value of the strong-interaction shift is quite limited. The accuracy of determining energy center value was at most ~ 2 eV [16] with SDDs, resulting in only exclusion of large shift and width. It has been known that a breakthrough improvement in energy resolution is essential to pin down the strong-interaction shift and width with a precision as good as ~ 0.2 eV (shift) and ~ 2 eV (width) respectively as it is predicted by many theoretical calculations [6, 17, 18].

With the aim of achieving these precisions, we have investigated a novel cryogenic detector, namely superconducting transition-edge-sensor (TES) microcalorimeter having a FWHM energy resolution of 5 eV at 6 keV. The instrument is a highly sensitive thermal sensor that measures an energy deposition by measuring the increase in the resistance of a superconducting material that is biased within the sharp phase transition between the normal and superconducting phases. The detailed working principles and the recent progress of the TES system are described in Refs. [19, 20]. Recent technological advances in multiplexed readout of a TES multi-pixel array (more than 100 pixel each having ~ 0.1 mm² effective area) allow performing a precision measurement in a realistic time interval.

Feasibility of hadronic-atom x-ray spectroscopy with TES spectrometer has been demonstrated in a hadron-beam environment similar to the secondary beamline in the J-PARC hadron hall. We successfully measured pionic carbon 4-3 x rays (~ 6.5 keV) with high resolution at a pion beamline of Paul Scherrer Institut (PSI) (see Section 3), and estimated necessary E17 beamtime to achieve the precision with realistic condition based on the PSI result (see Section 4).

We therefore update the precision goal of the present E17 experiment with an order of magnitude higher accuracy of determining the $2p$ level energy, i.e., 0.2 eV, both for kaonic- ${}^3\text{He}$ and kaonic ${}^4\text{He}$ atoms, by the use of TES microcalorimeter instead of employing SDDs. Moreover, direct measurements of the strong-interaction $2p$ -level widths become also possible for the first time, if its magnitude exceeds ~ 2 eV.

In parallel to the experimental study, we continued to discuss with several theoretical groups a possibility that our precise measurements provide information regarding the long-standing deep-shallow problem of \bar{K} -nucleus potential strength. Figure 2 (a) and (b) show preliminary calculation results [21], where the strong-interaction shifts and widths of $2p$ energy levels of kaonic- ${}^4\text{He}$ and kaonic- ${}^3\text{He}$ atoms were derived from the Klein-Gordon equation including QED corrections, assuming two different optical potentials of kaon-nucleus system based on Phenomenological Model [3] and Chiral Unitary Model [4]. In this calculation, they employed precise calculation results of charge density distributions for ${}^4\text{He}$ and ${}^3\text{He}$ newly calculated by the use of the Gauss expansion method [22]. Figure 2 (c) shows energy differences between kaonic- ${}^4\text{He}$ and kaonic- ${}^3\text{He}$ x rays for both potentials. The magnitude of the difference between the two Models was predicted to be ~ 0.6 eV. It should be noted that this comparison in Fig. 2 with our measurements both of kaonic- ${}^3\text{He}$ and ${}^4\text{He}$ atoms indicates that E17 experiment will add a fresh dimension to the study of \bar{K} -nucleus potential at zero energy and could lead to a settlement of the deep-shallow problem.

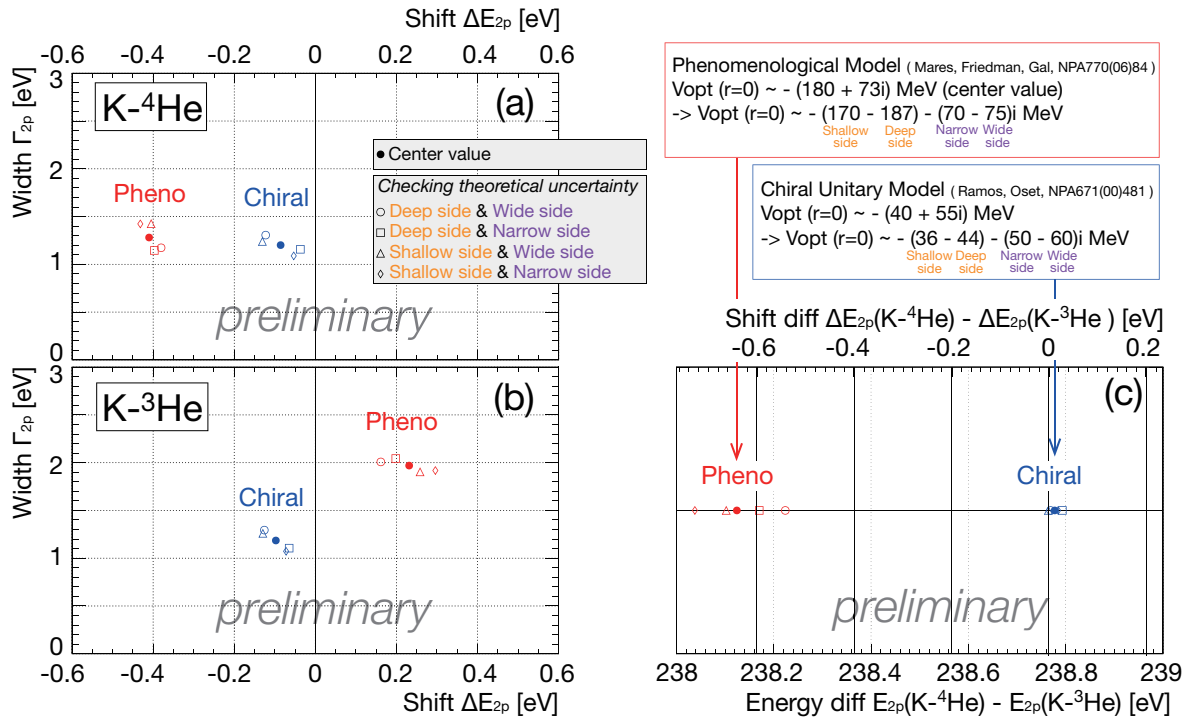


Figure 2: A preliminary result of the calculation of the strong-interaction shifts and widths of $2p$ atomic levels for kaonic ^4He (a) and kaonic ^3He (b) [21], assuming two different optical potentials of kaon-nucleus system based on Phenomenological Model [3] and Chiral Unitary Model [4]. Charge density distributions for ^4He and ^3He used here were newly calculated by the use of the Gauss expansion method [22]. The open symbols show the results for the real and imaginary potential strengths including the fit errors for Phenomenological Model and 10 % deviations for Chiral Unitary Model, respectively. (c) shows energy differences between kaonic- ^4He and kaonic- ^3He x rays for both potentials.

2 Experimental setup

The E17 experiment will be performed at the secondary beamline K1.8BR [25] in the hadron hall of J-PARC. Figure 3 shows the experimental setup. Incident kaons extracted with a momentum of 700 - 900 MeV/ c are counted with beamline counters, degraded in degraders, and stopped inside the liquid-helium target. X-rays emitted from the kaonic-helium atoms are detected by a TES spectrometer viewing the target from a side.

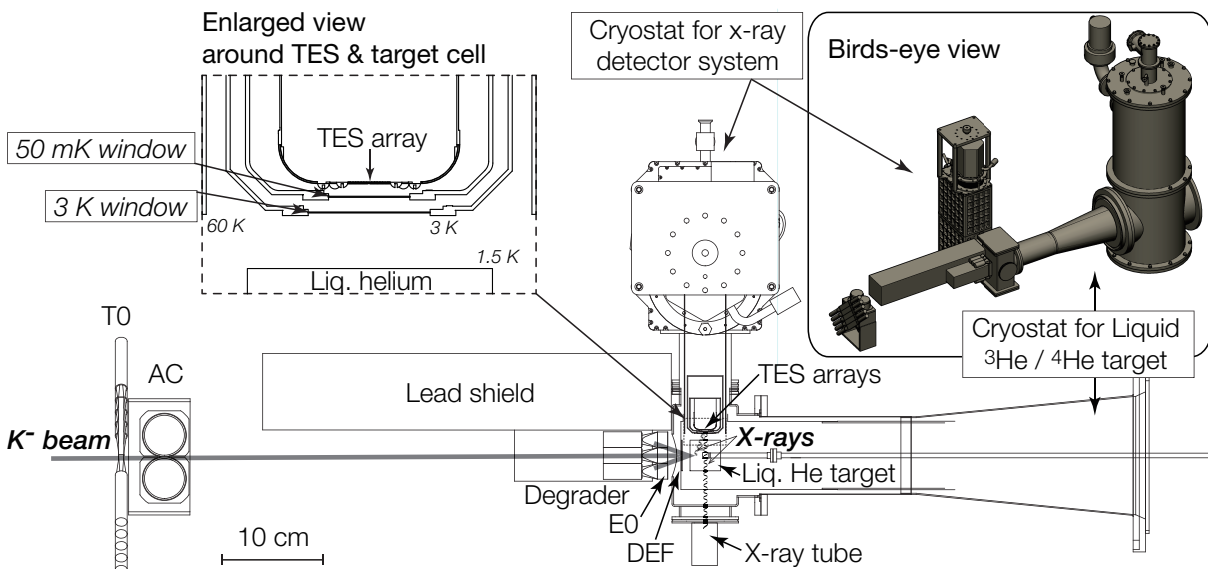


Figure 3: A cross-section top view of the E17 experimental setup around the experimental target. The insets show a birds-eye view and an enlarged view around TES and helium target cell. A set of beam detectors, a cryogenic liquid- ^3He and ^4He target system, and a NIST's TES x-ray spectrometer system are shown.

We do not employ tracking systems for secondary charged particles, because of difficulty in assuring enough coverage due to the cryogenic system for TES system, which leads to a reduction of kaonic x-ray yields.

2.1 TES microcalorimeter

We use a 240-pixel TES array designed for hard x-ray measurements developed by National Institute of Standards and Technology (NIST). Figure 4 (a) shows a photograph of the detector package. The array is on the top, where each pixel is wire-bonded for the readout time-division-multiplexing (TDM) chip mounted on each four sides. Figure 4 (b) shows a photograph of the 240-pixel array. Each TES consists of a superconducting bilayer of thin Mo and Cu films with an additional $4\text{-}\mu\text{m}$ thick Bi absorber [19]. The absorption efficiency of this Bi layer is about 80% for 6.5 keV x rays. Each pixel has an effective area of $320\ \mu\text{m} \times 300\ \mu\text{m}$, thus the total active area of the array is about $23\ \text{mm}^2$. TES array is collimated with a gold-coated $275\text{-}\mu\text{m}$ -thick silicon to avoid the unnecessary x-ray hit on the TES stage.

TESs are thermally isolated with the support of 100-nm thick silicon-nitride SiN_x membrane which limits the thermal conductance between TES and substrate. The sub-

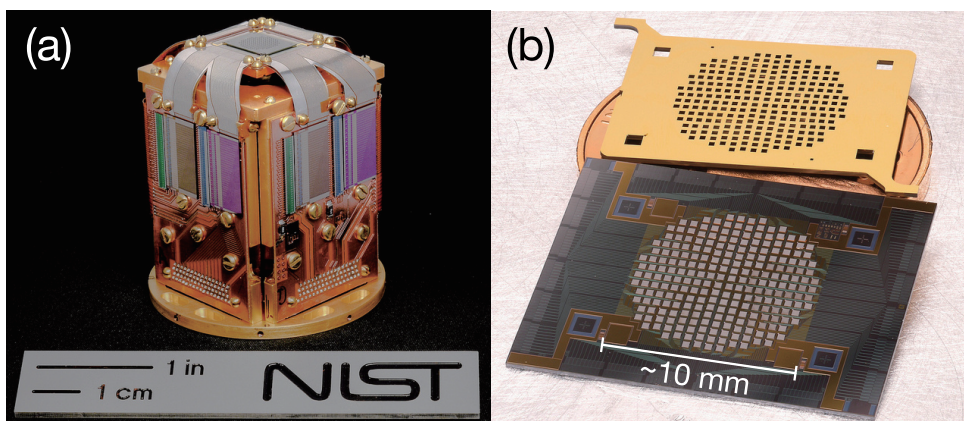


Figure 4: (a) A photograph of the detector package of the TES array. The array is on the top, where each pixel is wire-bonded for the readout TDM chip mounted on each four sides. (b) A photograph of the 240-pixel TES array. The gold-coated 275- μm -thick silicon collimator is stacked when installed. Photos credit: D.R. Schmidt, NIST.

strate is a grid structure of 275- μm -thick silicon wafer, the parts behind each TES are removed. A thermal heat sink layer of 500-nm-thick gold is deposited on the backside of substrate. This heat sink is connected to the low temperature thermal bath.

The TES array is operated at about 100 mK around the critical temperature, and is cooled with a pulse-tube-backed adiabatic demagnetization refrigerator (ADR). The pulse tube cools the system from 300K to 3K for 16 hours. Then 4-Tesla magnetic field is applied to the two-stage salt pills[§] through superconducting coils. By releasing the magnetic field adiabatically, the system is cooled down to 600 mK and finally to 75mK, which is regulated by a temperature controller. Temperature fluctuation is regulated about 7 μK (RMS) in the test experiment at PSI. The regulation hold time is 36 hours, after that the ADR cycle (magnetic field up and down) takes 3 hours. The initial set point of the TES temperature is decided by adjusting the TES resistance with applying bias voltage. The TES resistance is chosen to be the 20-30% of the normal resistance with optimizing the dynamic range and energy resolution.

The TES signal is read with the time division multiplexing (TDM) chip [26]. A TDM chip can read 30 channels in 9.6 μs (1 ch / 0.32 μs) by switching each SQUID, thus the sampling rate is 0.1 MHz for each channel. The 240 channels are read with 8 TDM chips in parallel. All TESs data are streamed in a PC server without any dead time, and only the self-triggered events are recorded. Figure 5 shows a typical recorded pulse of a pixel. The recorded number of samples is 1024 (=9.83 ms), the first 256 samples are pre-trigger data to define the baseline. In Fig.5, the baseline is already subtracted. The rise time is $\sim 200 \mu\text{sec}$, and the decay time is $\sim 500 \mu\text{sec}$.

[§]GGG: Gadolinium-Gallium Garnet, and FAA: Ferric-Ammonium Alum

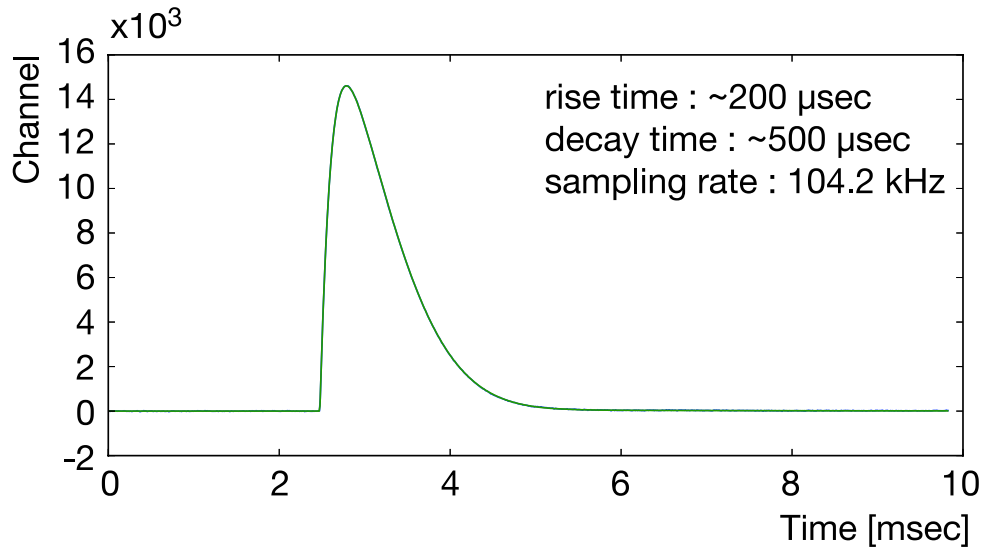


Figure 5: A typical recorded pulse of the TES with the time division multiplexing chip.

2.2 Energy calibration source

Precise energy calibration, performed with characteristic x rays whose energies, width and satellite peaks are well known, is crucial for a high-precision measurement. Since independent calibration is necessary for all 240 pixels, each with an effective area of $\sim 0.1 \text{ mm}^2$, it is essential to supply intense calibration x rays to achieve enough statistics for in-situ calibration.

In the E17 original proposal, we planned to use incident beam – mainly contaminating pions in the kaon beam – for activating fluorescent x-ray emission on pure metal foils; however, the beam-induced x-ray intensity, high enough for large detectors (like SDD), becomes insufficient for the a TES array, featuring small pixels. Thus, an x-ray tube generating a controllable flux of high-energy x rays will be installed, as we did in PSI, at the opposite side of TES x-ray spectrometer as shown in Fig. 3.

2.3 Liquid helium target system

A cryostat system for liquid- ^3He and ^4He at K1.8BR [25] will be used to cool down a cylinder-shaped target cell with a diameter of 6 cm and a length of 6 cm. The target volume, $\sim 170 \text{ cm}^3$, is reduced with respect to the original one ($\sim 500 \text{ cm}^3$, designed for SDDs), because the effective detection area of TES spectrometer is also reduced, requiring a different matching.

The superconducting TES array with a temperature of about 50 mK is located just beside the helium target cell with a temperature of 4 K; thus radiation-shield windows of 50 mK and 3 K are installed in between TES array and target cell as shown in the inset of Fig. 3. Therefore, some parts surrounding the target cell (e.g., 80 K radiation shield, vacuum jacket etc.) of the existing setup will be modified.

2.4 Trigger and data acquisition

The TES system acquires data continuously, in self-trigger mode. Since the x-ray signal has a latency of a few tens of μsec , the data-acquisition system for beam counters cannot wait for the TES response. Therefore, two independent data-acquisition systems are employed, for TES side and beam-counter side, respectively. The two systems are synchronized with a time stamp method involving dual information exchange: one, containing the kaon-stop timing is sent from the beam-trigger system to the TES data acquisition, while the other brings the 25-MHz clock signals of TES system to the beam-counter data-acquisition side with time-stamp information. Offline, an event-matching analysis will combine the two data sets.

The kaon-stop trigger, K_{stop} , will be given as follows :

$$\begin{aligned} K_{stop} &\equiv K_{beam} \otimes E0_{dE} \otimes \text{DEF} \\ K_{beam} &\equiv \text{BHD} \otimes \text{T0} \otimes \overline{\text{AC}} \end{aligned}$$

The elementary kaon-beam trigger, K_{beam} , is constructed by a coincidence signal from the following beam-line counters: BHD, T0, and AC. BHD[¶] and T0 are segmented plastic scintillation counters. AC is an aerogel Cherenkov counter with a reflective index of 1.05, which reduce π^- contamination in the beam. The kaon-stop trigger is, then, constructed by an additional coincidence signal from the beam definition counter (DEF) and the dE/dX counter (E0). The threshold for E0 will be optimized to select large energy depositions by almost stopping kaons.

[¶]BHD is located upstream of the K1.8BR beam line spectrometer [25].

3 Demonstration of TES operation at pion beamline

3.1 Experimental setup

The TES x-ray spectrometer has never been used in hadron-beam environment. To demonstrate the functioning in a hadron-beam environment similar to the secondary beamline in the J-PARC hadron hall, the HEATES collaboration^{||} has tested the in-beam performance of the spectrometer, by measuring pionic x rays at PSI π M1 beamline [24] recently (27 October - 5 November, 2014).

Figure 6 shows the experimental setup. Incident π^- 's extracted with a momentum of ~ 170 MeV/ c are degraded in moderators, counted with beamline counters, and stopped in a carbon graphite target. Pionic- ^{12}C $4f-3d$ x rays (~ 6.5 keV) are detected by the superconducting TES spectrometer located aside the target. To provide the characteristic x rays for energy calibration, an X-ray tube that can generate high-energy x rays was installed at the opposite side of TES x-ray spectrometer.

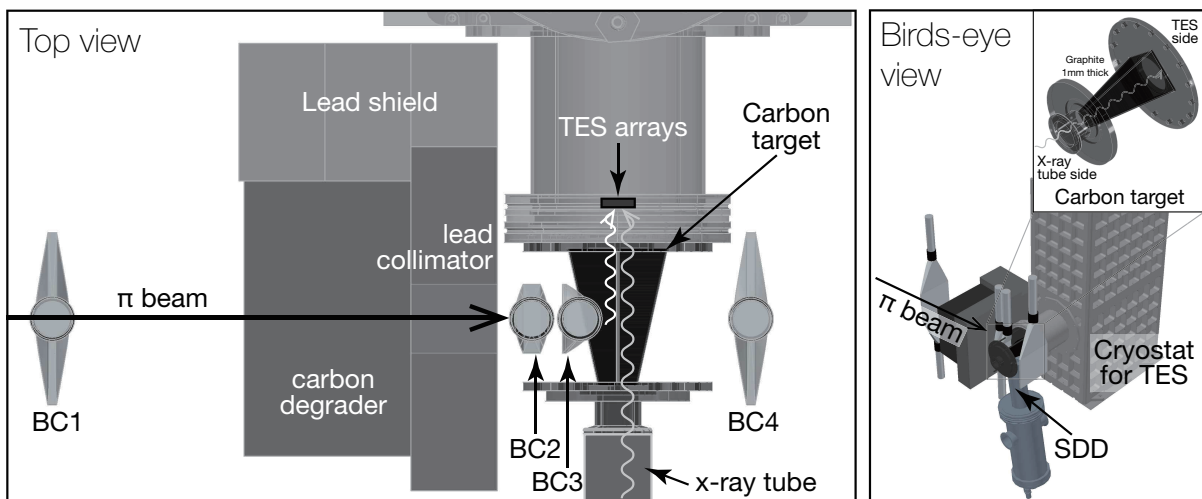


Figure 6: A top view (left) and birds-eye view (right) of the beam-test setup at PSI.

3.2 Results of pionic-carbon 4-3 x-ray measurement

Figure 7 shows an x-ray energy spectrum measured with the x-ray tube shining the Cr and Co calibration foils with beam-off condition at the PSI beamline. Four x-ray lines, Cr K_α , Cr K_β , Co K_α , and Co K_β , are used for energy calibration with cubic spline interpolation. In the spectral fitting, energies and natural widths of all calibration lines are fixed with the reference values [27]. Lower-yield x rays, Fe K_α (6.4 keV) and Cu K_α (8.0 keV), originate respectively from surrounded stainless steels and Cu inside of the detector package. The Fe K_α line is useful to estimate the accuracy of energy calibration. A fit of the Fe K_α line in the summed spectrum of all available pixels gives a FWHM energy resolution of 4.6 eV at 6.4 keV.

Figure 8 shows the preliminary results of (a) a correlation plot of the time difference between pion arrival and x-ray detection with TES versus x-ray energy measured by the

^{||}The HEATES collaboration [23] is formed to drive forward “High-resolution Exotic Atom x-ray spectroscopies using TES microcalorimeters” and is included a part of E17 member.

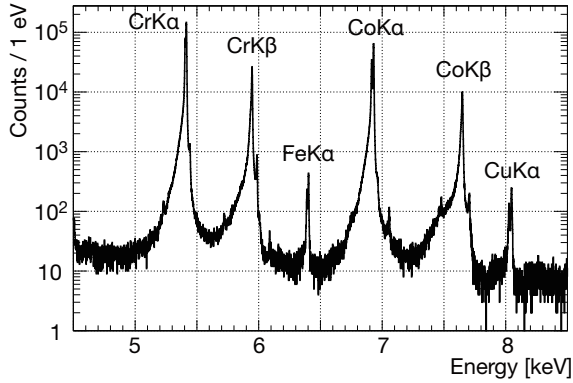


Figure 7: An x-ray energy spectrum measured with an x-ray tube shining the Cr and Co calibration foils in beam-off condition. The Cr K_α , Cr K_β , Co K_α , and Co K_β lines are used for the energy calibration. Lower-yield x rays, Fe K_α (6.4 keV) and Cu K_α (8.0 keV), originate respectively from surrounded stainless steels and Cu inside of the detector package.

TES array, (b) the projection on the time axis, (c) the projection on the energy axis by selecting stopped- π^- time gate indicated in the time spectrum, and (d) an x-ray energy spectrum of a SDD used as a reference in this experiment. A fit of the energy spectrum gives a FWHM energy resolution of 7.2 eV at 6.4 keV with beam-on condition. A time resolution is obtained to be $\sim 1.2 \mu\text{sec}$ with which the timing cut improved a signal-to-noise ratio in energy spectrum from 2 to 10. At around 6.43 keV, a sharp peak from the pionic-carbon $4f \rightarrow 3d$ transition together with its parallel transition $4d \rightarrow 3p$ was successfully observed with a clear timing correlation with the beam. The x-ray tube has been turned on during the data taking and weakly shines surrounded materials containing iron; thus Fe $K_{\alpha 1}$ (6.404 keV) and Fe $K_{\alpha 2}$ (6.391 keV) lines are observed uncorrelated with beam timing. The major parameters of those plots in Fig.8 summarized below:

Data acquisition	: ~ 13.5 hours
Beam rate (BC1 rate)	: 1.45 MHz (with 2.2 mA of primary proton)
Stopped π^- trigger rate	: 34.5 kHz
x-ray tube	: ON with calibration foils of Cr & Co
TES hit rate	: 4.8 Hz/pixel of which 0.4 Hz is due to beam
Selected TES pixel	: 213 pixels
Analysis efficiency	: 80% (rejected events : pileup 4% + thermal crosstalk 16%)

A preliminary spectral fit result of Fe K_α and pionic carbon lines is shown in Fig. 8 (c). The energy-calibration accuracy is assessed by the fit result of Fe K_α line. Resulting energy of Fe $K_{\alpha 1}$ is

$$6404.07 \pm 0.10(\text{stat.})_{-0.04}^{+0.06}(\text{syst.}) \text{ eV (preliminary)}$$

where the first error is statistical and the second is systematic. The quoted systematic error is a quadratic summation of the contributions from continuum background parameter and asymmetry of the fit function. A comparison with the reference value of 6404.148(2) eV [27] shows a good agreement within errors. The energy-calibration accuracy is therefore evaluated to be less than ± 0.1 eV.

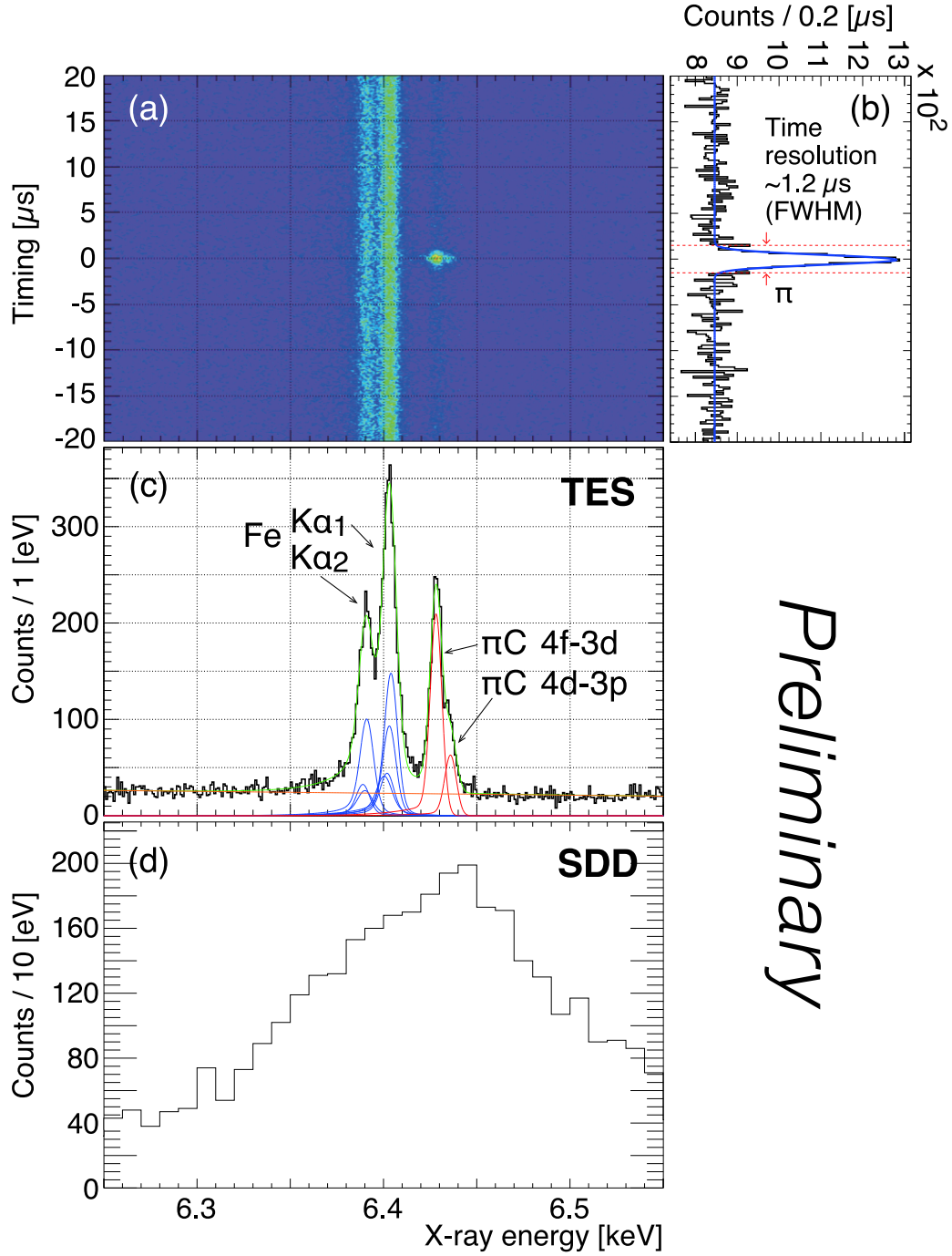


Figure 8: Preliminary results of the measured x-ray time and energy distributions for stopped- π^- trigger events. (a) A correlation plot of the time difference between pion arrival and x-ray detection vs the x-ray energy measured by the TES array. (b) The projection on the time axis. (c) The projection on the energy axis by selecting stopped- π^- time gate indicated in (b), where fit components for Fe K_α and pionic-carbon x rays are shown as well. (d) An x-ray energy spectrum measured by the reference SDD having a FWHM energy resolution of ~ 165 eV.

3.3 Effects due to charged-particle hit on TES system

We observed that the energy resolutions of TESs operated with beam-on condition are deteriorated, which linearly correlates with the charged-particle hit rate on TESs, i.e., beam intensity. Figure 9 shows a correlation plot of an averaged charged-particle hit rate per pixel versus an energy resolution at 6.4 keV obtained by a fit of Fe K_α peak in the summed spectrum of all available pixels. The charged-particle hit rate is defined as the remainder of difference between a total hit rate of TES with beam-on condition and a hit rate due to calibration x-ray hits which is estimated with beam-off condition (~ 4.4 Hz/pixel) where the x-ray tube is operated with the same condition. This rate is proportional to the beam intensity.

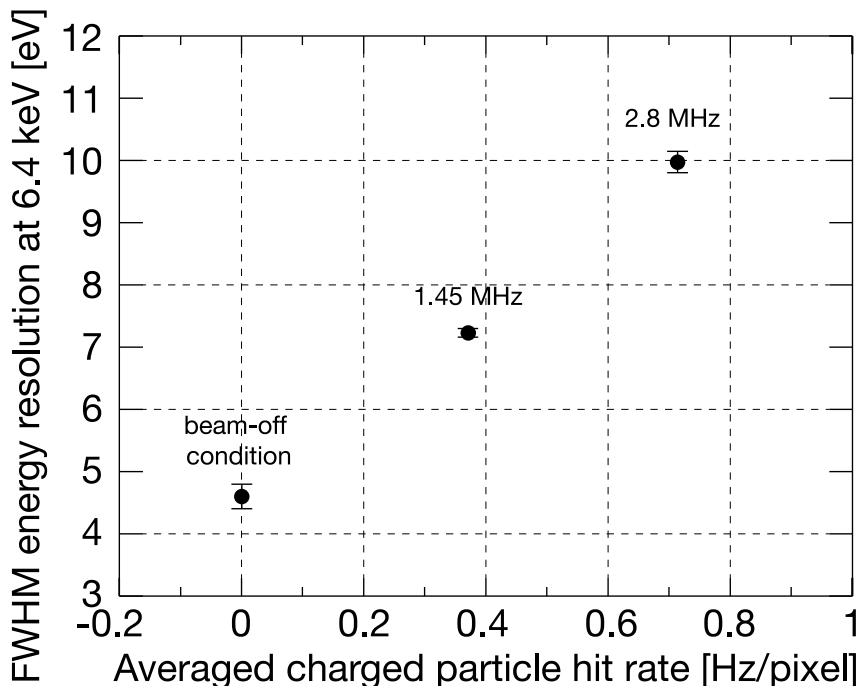


Figure 9: A correlation plot of averaged charged-particle hit rates per pixel versus FWHM energy resolutions at 6.4 keV estimated with a Fe K_α x-ray peak

We have investigated the causes of the resolution deterioration through the detailed pulse-shape analysis of TESs which themselves are useful as the most sensitive temperature sensors to examine the charged-particle hit effects. It is revealed that a temperature rise due to a large energy deposition by a charged-particle hit on TESs and/or its support structures affects not only local pixels but also whole array.

The blue plot of Fig. 10 (a) represents relative pulse heights of several TESs within a typical event where a number of pixels triggered at the same timing. The abscissa corresponds to the actual geometrical distance from a charged-particle hit position. The hit position is assumed to be a position of a pixel having the largest pulse height among them. The green line represents a calculation result of temperature rise which corresponds to TES pulse height, where the thermal diffusion in the silicon substrate and the conductance to the heat bath are taken into account.

Figure 10 (b) shows a schematic drawing of TES-array cross section. The most influ-

ential events are expected to be when charged particles deposit their energies on 275- μm -thick silicon substrate (up to a few MeV). A heat generated by a charged-particle hit is diffused and attenuated within several micro second through the silicon substrate. This time scale is much faster than the milli-second TES response.

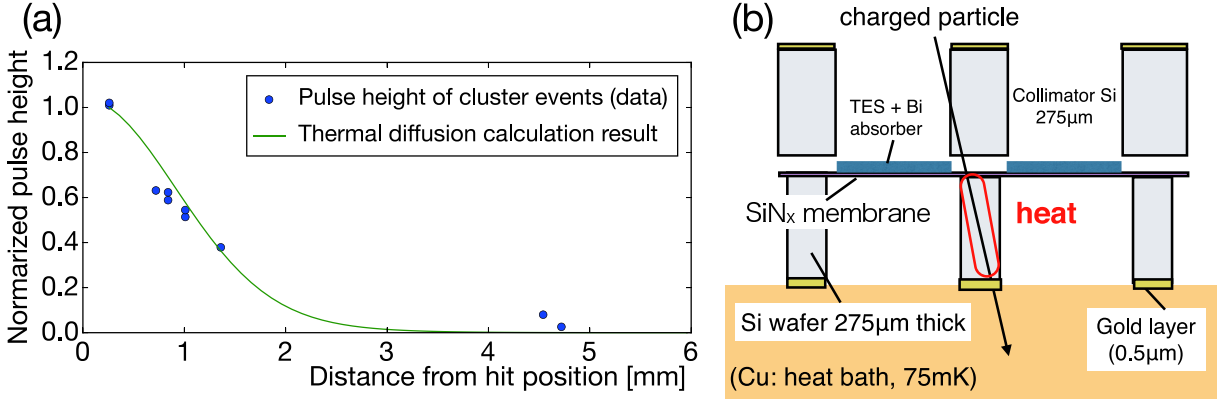


Figure 10: (a) Blue plot shows relative pulse heights of several TESs within a typical event as a function of the actual geometrical distance from an assumed charged-particle hit position. Green line represents a calculation result of temperature rise, where the thermal diffusion in the silicon substrate and the conductance to the heat bath are taken into account. (b) Schematic drawing of TES-array cross section. An event where a charged-particle penetrates a thick silicon substrate of the array is shown.

When a charged-particle hit is coincident with an x-ray hit in any of TESs, the heat flowed from the silicon substrate and the SiN_x membrane creates a bump in the time-stream of x-ray pulse. This is a so-called thermal crosstalk. Figure 11 shows typical x-ray pulses having the thermal crosstalks. The bump structure affects the pulse height which is determined by filtering the signal pulse with the averaged pulse. After eliminating detectable pileup events, remained tiny thermal-crosstalk bumps will distort the pulse and change the pulse height a bit comparably with noise and thermal fluctuation, which results in the deterioration of energy resolution.

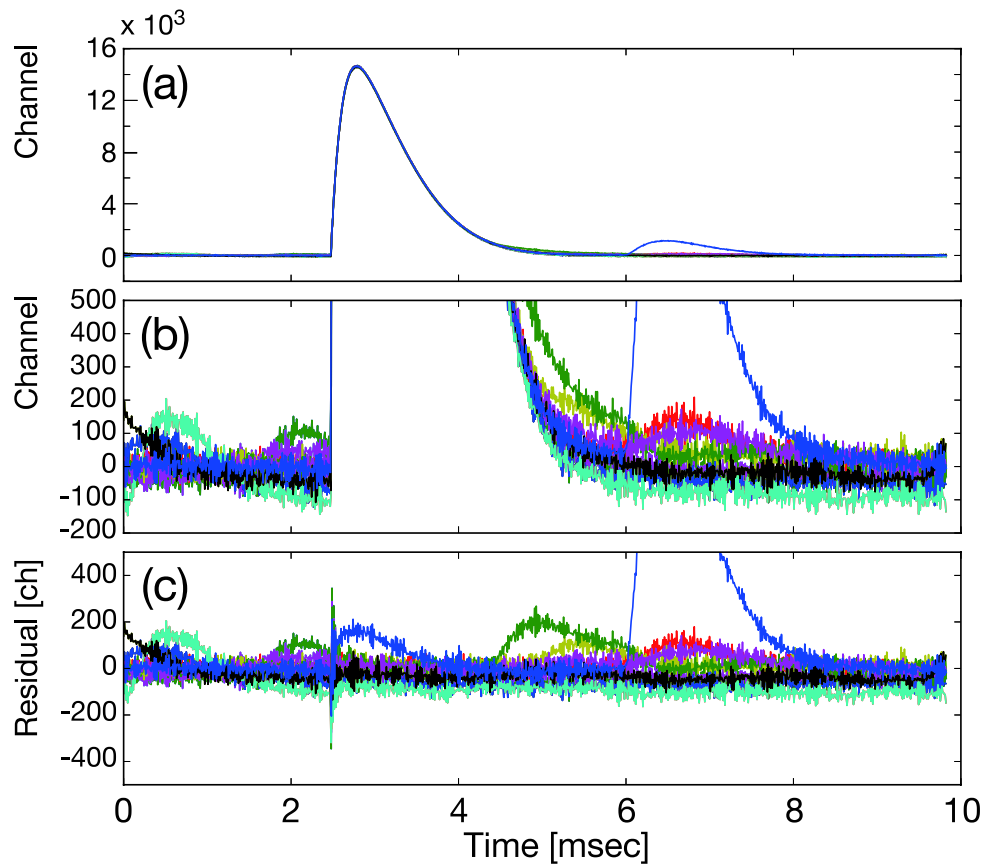


Figure 11: (a) Typical Cr K_{α} x-ray pulses with thermal crosstalks. (b) Enlarged view of the same histograms as (a). (c) Residuals from the averaged pulse, where the baselines are already subtracted. Tiny crosstalk bumps distort the pulse shapes which affects the pulse height determination.

4 Monte-Carlo study of K^- beamline at J-PARC

4.1 Yield estimation of the kaonic atom x-rays

To estimate and maximize the kaonic-atom x-rays yield a Monte-Carlo simulation study was performed using Geant4 toolkit**. First, the thickness of the degrader was optimized to maximize the number of stopped K^- events in the helium target, where measured K^- beam properties are used as input parameters. The acceptance of the TES spectrometer was then assessed using the stopped K^- distribution obtained. The optimized parameters and other factors assumed for the yield estimation are summarized as follows:

Incident secondary-beam momentum at K1.8BR beamline	: 0.9 GeV/ $c^{\dagger\dagger}$
Kaon beam intensity @ T0	: 3.2×10^3 counts/spill/kW
Total intensity (mostly π^-) @ T0	: 1.6×10^4 counts/spill/kW
Liquid helium target cell size (cylinder)	: ϕ 6 cm \times 6 cm (~ 170 cm ³)
Mixture ratio of liquid ^4He and ^3He	: 2 : 1
K^- stop efficiency	: 0.08
Distance from beam center to TES face	: 5 cm
TES acceptance (including attenuation)	: 0.028 %
Reduction factor due to hold time (ADR & liquid He filling)	: 0.9
Beam-line DAQ & trigger efficiency	: 0.9
TES good pixel ratio	: 0.9
Analysis efficiency	: 0.9
Kaonic helium $3d \rightarrow 2p$ yield per stopped K^-	: 7.5 %

We employ a mixed ^3He and ^4He gas which already exists. The amount of mixed ^3He gas is limited, which results in the ^4He and ^3He mixture ratio of 2 : 1. In the present estimation, the x-ray yields from kaonic ^4He and ^3He atoms are 240 and 120 counts, respectively, with 100 kW·week beam time.

4.2 Estimation of the charged-beam background

One of the most important concerns is whether the TES spectrometer works with a good energy resolution in the kaon-beam environment. Assuming the slow-extraction beam power of 50 kW, we expect a total beam intensity of 8×10^5 per spill at 0.9 GeV/ c . This intensity is much smaller than we had in the PSI experiment; however the beam particle and the beam momentum are different. Therefore we evaluated the charged-particle hit rate on TES absorbers and a silicon structure behind them, which should strongly correlate with the energy-resolution deterioration as shown in Fig. 9. For reproducibility check of the simulation method, we performed simulation studies not only for the proposed kaon experiment with E17 setup but also for the PSI experiment.

Figure 12 shows a comparison of energy spectra between PSI data and the simulation results. The experimental data was taken for ~ 3 hours with a total beam intensity of

**Geant4 toolkit : version 4.10.00.p02 with a physics list of QGSP_BERT for hadron physics and G4EmStandardPhysics_option4 for electromagnetic interaction

$\dagger\dagger$ A beam momentum of 0.9 GeV/ c results in a better K^- stop efficiency in the simulation assuming beam intensities obtained by the past beam measurements. However, the actual beam momentum will be determined by a K^- -stop tune run that we requested as a beam-commissioning before production run.

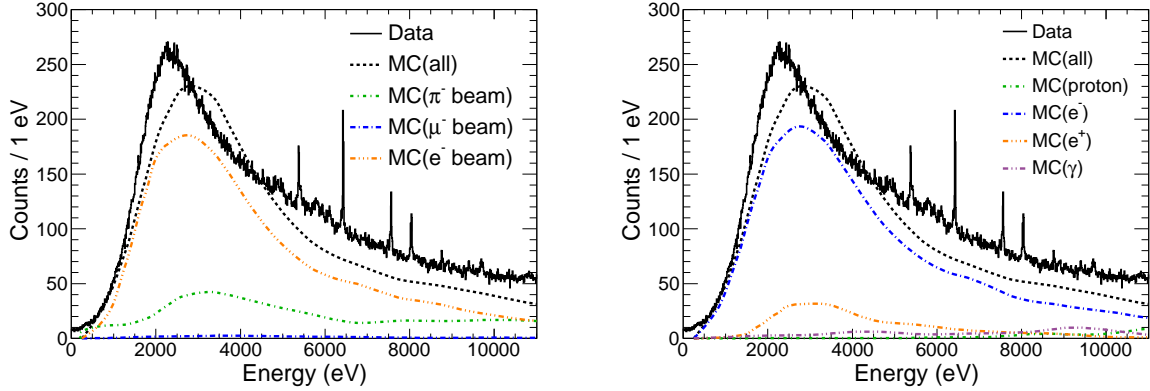


Figure 12: Measured TES self-triggered energy spectrum obtained at PSI experiment with beam-on and no calibration x-ray (x-ray tube off) conditions, compared with the simulated spectra. The left and right panels include different disaggregated data with initial beam particles (left) and particle species hitting on the TES (right), respectively.

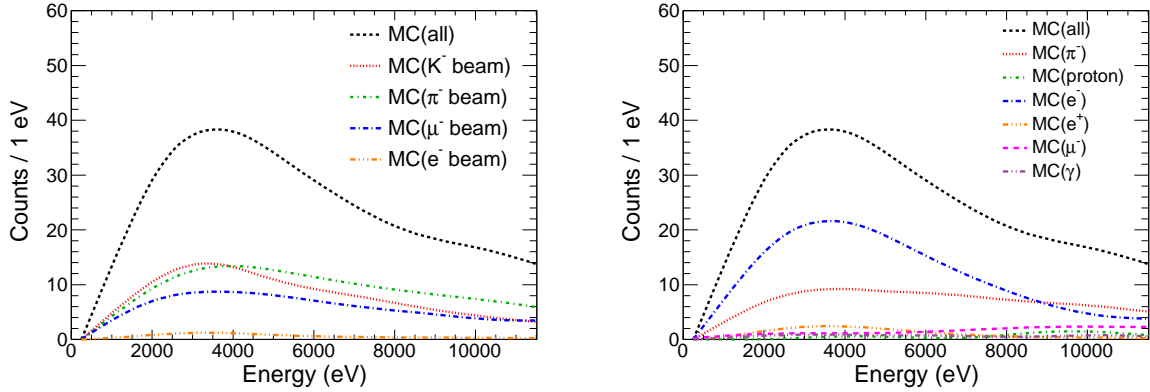


Figure 13: Simulated TES self-triggered energy spectrum with J-PARC E17 condition for 1-day data taking. The left and right panels include different disaggregated data with initial beam particles (left) and particle species hitting on the TES (right), respectively.

2.8×10^6 /sec without calibration x rays (x-ray tube off condition). The spectrum contains therefore only the events induced by beam. It should be noted that this beam intensity was twice higher than that in the measurement described in Section 3.3 because of a wider slit setting. The simulated spectrum was normalized by the number of incident beam, where a flux ratio among the incident beam particles was determined by data measured with TOF method. The simulation indicates that the background mostly comes from electrons hitting on TESs. Minimum ionization particles (MIPs) unfortunately give energy deposits on the TES absorber ($4\text{-}\mu\text{m}$ -thick Bi) in the region of interest (~ 6 keV); thus direct hits of MIPs on the absorber could be a dominant background. The trigger rate of TES was estimated to be 0.64 /sec, whereas the experimental result is 0.71 ± 0.11 /sec. With the good reproducibility of the hit rate and the spectral shape, we applied this simulation method to kaon-beam environment at J-PARC.

Figure 13 shows background spectra in the case of J-PARC E17 condition. Table 1 summarizes the major input parameters of the beam condition and resultant TES trigger

Table 1: Major input parameters for the simulations. The particle hit rates on the TES system obtained from the simulations are shown as well. Note that the rates at J-PARC is normalized by spill whose typical length is 2 seconds.

	π M1 at PSI	K1.8BR at J-PARC
Beam momentum	173 MeV/ c	900 MeV/ c
Total beam intensity	2.8×10^6 /sec	8.0×10^5 / spill
$K^-/\pi^-/\mu^-/e^-$ ratio	—/ 40% / 5% / 55%	20% / 60% / 10% / 10%
TES trigger rate / pixel	0.64/sec	0.27 /spill
Energy deposit on Si	152 MeV/sec	87 MeV/spill

rates both for PSI and J-PARC cases. The last row in the table shows the energy deposition rates on the silicon substrate evaluated in the same framework. The comparison between PSI and J-PARC cases indicates that the condition we operated TES at PSI was more severe than the condition at J-PARC. Note that the trigger rates at J-PARC is normalized by spill whose typical length is 2 seconds. Assuming the phenomenological relation concerning resolution deterioration with charged-particle hit rate as shown in Fig. 9, we expect that in J-PARC E17, the TES spectrometer should work with a FWHM energy resolution of better than 6 eV at 6 keV.

4.3 Estimation of the background in the final spectrum

Signal-to-background ratio is crucial for the precision spectroscopy of kaonic-atom x-rays due to their relatively low yields. Because the ratio is defined by the energy width of the detector intrinsic resolution, the excellent resolution of TES naturally improves the ratio. On the other hand, as stated in the Section 4.2, the direct-hit events of MIPs on the TES absorber will directly contribute to the continuum background unlike SDDs where the large energy deposits given by MIPs are out of the region of interest.

Two kinds of continuum-background component are expected in the final spectrum after K^- -stop timing selection. One is asynchronous background which comes randomly without generating stopped K^- trigger, the other is synchronous background correlating with the trigger timing.

Asynchronous background is proportionally reduced by the occupation ratio of the stopped- K^- timing window. With the assumptions listed in Table 2, the occupation ratio is estimated to be 4.5×10^{-3} . Most of the backgrounds shown in Fig. 13 is the asynchronous background. The background yield without stopped- K^- trigger at 6 keV is 30 counts / eV / day. Therefore, the asynchronous background in J-PARC setup is estimated to be 2 counts / eV during 2-week data taking with 50 kW beam power.

Synchronous background is expected to be significant in J-PARC. This originates from the in-flight- and stopped- K^- reaction on the materials around the target. Especially in the K^- absorption processes, even after the emission of the kaonic atom x-rays, secondary charged particles are energetically produced via hyperon productions and their decays. The synchronous background in J-PARC setup is estimated to be 6 counts / eV. This mainly comes from the K^- reactions at the target cell and various radiation shields.

As a result, the total background yield is estimated to be 8 counts / eV (= 2 (asyn-

Table 2: Occupation ratio of the stopped- K^- timing window and its assumptions

Online stopped- K^- trigger rate (R_{K^-})	3×10^3 / spill
Spill length (L_{spill})	2 seconds
Offline trigger-purification factor ($F_{offline}$)	0.5
TES timing gate width (W_{gate})	$3 \mu\text{s}$ / trigger
Duty factor (F_{duty})	0.5
Occupation ratio ($= R_{K^-} / L_{spill} \times F_{offline} \times W_{gate} / F_{duty}$)	4.5×10^{-3}

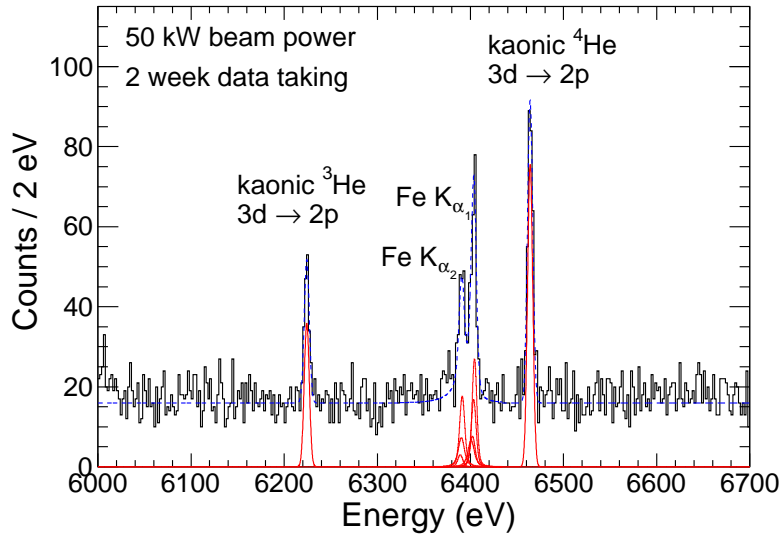


Figure 14: Simulated x-ray energy spectrum of $3d \rightarrow 2p$ transitions in kaonic ^3He and ^4He atoms with J-PARC E17 setup for 2-weeks data taking with 50 kW beam power. The expected calibration lines of Fe $K_{\alpha 1}$ and $K_{\alpha 2}$ are also shown, which is completely separated from kaonic-helium lines and the intensity of calibration lines is controllable by adjusting the current and voltage values of x-ray tube.

chronous) + 6 (synchronous)) for 2-week data taking with 50 kW beam power.

Figure 14 shows an estimated x-ray energy spectrum of $3d \rightarrow 2p$ transitions in kaonic ^3He and ^4He atoms with J-PARC E17 setup for 2-weeks data taking with 50 kW beam power (100 kW-weeks) with the following evaluated yield and background: the kaonic-atom x-ray yields of 240 counts (K^- - ^4He) and 120 counts (K^- - ^3He), and the constant background of 8 counts / eV. When we assume an energy resolution of 6 eV FWHM and the natural widths of 0 eV, the statistical accuracies of determining the energy with the expected background yield for kaonic ^3He and ^4He would be respectively ± 0.35 eV and ± 0.2 eV, where the systematic error is expected to be ± 0.1 eV as stated in Section 3.2.

5 Beam time request

We request a beamtime of 100 kW·week for production run, e.g., two weeks with a beam intensity of 50 kW. For commissioning runs, we request 3 days for K^- stop tune, and 4 days for full commissioning with TES spectrometer. Our run plan and beam time request are summarized as follows:

K^- stop tune	3 days
Full commissioning with TES spectrometer	4 days
Production run	100 kW·weeks

6 Time schedule and cost estimation

The summary of intended time schedule of the proposed experiment is shown in Fig.15. We are going to purchase a new ADR, the refrigerator system for TES, which is the same model as what we used in PSI experiment. With the new ADR, we employ an identical x-ray detection system used in the PSI experiment as introduced in Section 3. We will finish the commissioning of TES system together with liquid-helium target system (without beam) by May 2016 and will be ready for data taking on June 2016.

We wish to perform a K^- -stop tune well before the production run, since the tune do not require the readiness of TES system and is important for confirmation of the K^- -stop rate estimated above.

In table 3, we summarized a list of equipment items and its costs for the proposal experiment.

Year	2015							2016					
Month	6	7	8	9	10	11	12	1	2	3	4	5	6
TES system	fabrication of ADR				assemble			performance evaluation test			commissioning		ready for data taking
Target cell	design	fabrication		test for each components			assemble	performance evaluation test					
Trigger detectors	design		fabrication		performance evaluation test								

Figure 15: Schedule of preparation of the proposed experiment

Item	Cost[kJY]	Comments
X-ray detection system		
An array of Transition-Edge Sensor (240 pixel)	—	existing
SQUID multiplexer chips and interface chips	—	existing
Series-array SQUID modules	—	existing
Electronics and DAQ system	—	existing
Adiabatic Demagnetization Refrigerator (ADR)	25,000	Grant-In-Aid (granted)
Mechanical parts - 50 mK “snout”	—	existing
Mechanical parts - other than 50 mK “snout”	1,800	Grant-In-Aid (granted)
X-ray calibration system		
X-ray tube	—	existing
Calibration foils	—	existing
Target system		
Cryostat system	—	existing
Liquid Helium 3 and 4	—	existing
Target cell with beryllium windows	500	Grant-In-Aid (granted)
Vacuum chamber and its support	2000	Grant-In-Aid (granted)
Beamline detector system		
Trigger counters (Aerogel, T0, Veto counters)	—	existing
Degraders	—	existing
Electronics		
NIM, VME modules	—	existing
Rack, Bin, Crate etc.	—	existing
DAQ system	—	existing
Analysis computer system	—	existing
Data storage	—	existing

Table 3: Estimated cost

References

- [1] M. Bazzi, *et al.* (SIDDHARTA Collaboration), Phys. Lett. B **704** (2011) 113;
M. Bazzi, *et al.* (SIDDHARTA Collaboration), Nucl. Phys. A **881** (2012) 88.
- [2] Y. Ikeda, T. Hyodo, W. Weise, Phys. Lett. B **706** (2011) 63;
Y. Ikeda, T. Hyodo, W. Weise, Nucl. Phys. A **881** (2012) 98.
- [3] J. Mareš, E. Friedman, A. Gal, Nucl. Phys. A **770** (2006) 84.
- [4] A. Ramos, E. Oset, Nucl. Phys. A **671** (2000) 481.
- [5] C.J. Batty, E. Friedman, A. Gal, Phys. Reports **287** (1997) 385.
- [6] S. Hirenzaki, Y. Okumura, H. Toki, E. Oset, and A. Ramos, Phys. Rev. C **61**, 055205 (2000).
- [7] M. Agnello *et al.*, Phys. Rev. Lett. **94**, 212303 (2005).
- [8] T. Yamazaki *et al.*, Phys. Rev. Lett. **104**, 132502 (2010).
- [9] Y. Ichikawa *et al.*, Prog. Theor. Exp. Phys., 021D01 (2015).
- [10] S. Baird *et al.*, Nucl. Phys. **A392**, 297 (1983).
- [11] Y. Akaishi, proceedings for *International Conference on Exotic Atoms (EXA05)*, Austrian Academy of Sciences Press, Vienna, 2005, p. 45.
- [12] R. S. Hayano *et al.*, Proposal of J-PARC E17 (2006)
http://j-parc.jp/researcher/Hadron/en/Proposal_e.html#0606.
- [13] R. S. Hayano *et al.*, “E17/E15 status” presentation at the 9th J-PARC PAC meeting
http://nuclpart.kek.jp/pac/1001/J-PARC_PAC9.html.
- [14] M. Bazzi, *et al.* (SIDDHARTA Collaboration), Phys. Lett. B **697** (2011) 199.
- [15] M. Bazzi, *et al.* (SIDDHARTA Collaboration), Phys. Lett. B **681** (2009) 310.
- [16] S. Okada, *et al.*, Phys. Lett. B **653** (2007) 387.
- [17] C. J. Batty, Nucl. Phys A **508** (1990) 89c.
- [18] E. Friedman, talk at EXA 2011: <https://indico.gsi.de/materialDisplay.py?contribId=56&sessionId=17&materialId=slides&confId=1221>.
- [19] K.D. Irwin and G.C. Hilton, “Transition-Edge Sensors”, C. Enss (ed.), Cryogenic Particle Detection, Topics in Applied Physics, vol. **99**, Springer, 2005.
- [20] D.A. Bennett *et al.*, Rev. Sci. Instrum. **83** (2012) 093113.
- [21] J. Yamagata-Sekihara and S. Hirenzaki, Private communication.
- [22] E. Hiyama, Private communication.

[23] The HEATES collaboration :

D.A. Bennett^a, C. Curceanu^b, W.B. Doriese^a, J.W. Fowler^a, J. Gard^a, F.P. Gustafsson^c, T. Hashimoto^d, R.S. Hayano^e, S. Hexi^b, M. Iliescu^b, S. Ishimoto^f, K. Itahashi^d, M. Iwasaki^d, K. Kuwabara^g, J. Marton^h, H. Noda^d, G.C. O'Neil^a, S. Okada^d, H. Outa^d, C.D. Reintsema^a, M. Sato^d, D.R. Schmidt^a, K. Suzuki^h, T. Suzuki^e, D.S. Swetz^a, H. Tatsuno^{b,f}, J. Uhlig^c, J.N. Ullom^a, E. Widmann^h, S. Yamada^g, J. Zmeskal^h

^a National Institute of Standards and Technology, 325 Broadway, Boulder, CO 80303, USA

^b INFN, Laboratori Nazionali di Frascati, Via E. Fermi 40, Frascati, RM, I-00044, Italy

^c Lund University, Box 117, 221 00 Lund, Sweden

^d RIKEN Nishina Center, RIKEN, 2-1 Hirosawa, Wako, Saitama, 351-0198, Japan

^e The University of Tokyo, 7-3-1 Hongo, Bunkyo-ku, Tokyo 113-0033, Japan

^f High Energy Accelerator Research Organization, KEK, 1-1 Oho, Tsukuba, Ibaraki, 305-0801, Japan

^g Tokyo Metropolitan University, 1-1 Minami-Osawa, Hachioji, Tokyo, 192-0397, Japan

^h Stefan-Meyer-Institut für subatomare Physik, Boltzmanngasse 3, Vienna, 1090, Austria

[24] PSI π M1 beamline: http://aea.web.psi.ch/beam2lines/beam_pim1.html.

[25] K. Agari *et al.*, Prog. Theor. Exp. Phys. (2012) 02B011.

[26] J.A. Chervenak *et al.*, Appl. Phys. Lett. **74**, (1999) 4043.

[27] G. Hölzer *et al.*, Phys. Rev. A. **56** (1997) 4554.

Appendix

J-PARC E17 original proposal

Executive summary of E17 original proposal

We propose to measure the strong-interaction shift of $3d \rightarrow 2p$ X-rays of kaonic helium 3 atoms with a precision better than 2 eV at the J-PARC 50-GeV PS. The proposed experiment, analyzed together with that for kaonic helium 4 atoms measured by the KEK-PS E570 collaboration [1], will provide crucial information on the isospin-dependent \bar{K} -nucleus strong interaction at the low energy limit, and will provide decisive data to understand the basis of the Akaishi-Yamazaki prediction of deeply-bound kaonic nuclei [2], and to clarify the nature of the strange multibaryon candidates recently reported at KEK [3], DAΦNE [4] and BNL [5]. The major parameters of the proposed experiment are summarized below:

Reaction	: stopped $K^- + {}^3\text{He} \rightarrow h\nu(\sim 6.4\text{keV}) + X$
Primary beam	: 30 GeV, 9 μA proton
Secondary beam	: 0.75 GeV/c K^-
Beamline	: K1.8BR or K1.1
Target	: Liquid ${}^3\text{He}$, diameter 6.4 cm, length 15 cm (482.5 cm ³)
Detectors	: $8 \times 100 \text{ mm}^2$ silicon drift detectors (SDD), beamline counters and chambers, vertex trigger counters and tracking chambers.
Beam time	: 10 days for commissioning +3.5 days at K1.8BR (assuming full PS intensity) +35 days at K1.8BR (with 10% of the design intensity) ^a

The present proposal is closely related to another proposal to the J-PARC 50-GeV PS, “A search for deeply-bound kaonic nuclear states by in-flight ${}^3\text{He}(K^-, n)$ reaction” [6]. Both of these experiments address the question of deeply-bound kaonic states, and there is a large overlap of the collaboration members. Both experiments will use the same beamline and the same ${}^3\text{He}$ target. In view of the relative simplicity of the X-ray measurement and its modest beam requirement, we believe it is appropriate to execute the present X-ray proposal before the “in-flight” experiment. The proposed experiment will be ready on DAY-1, and can quickly deliver crucial physics results. It is hence most suited as the J-PARC DAY-1 experiment.

References

- [1] R. S. Hayano *et al.*, Proposal of KEK-PS E570 (2005).
- [2] Y. Akaishi and T. Yamazaki, Phys Rev. **C65**, 044005 (2002) .
- [3] T. Suzuki *et al.*, Phys. Lett. **B597**, 263-269 (2004).
- [4] M. Agnello *et al.*, Phys. Rev. Lett. **94**, 212303 (2005).
- [5] T. Kishimoto *et al.*, Nucl. Phys. A **754**, 383c (2005).
- [6] M. Iwasaki *et al.*, Proposal of J-PARC 50-GeV PS “A search for deeply-bound kaonic nuclear states by in-flight ${}^3\text{He}(K^-, n)$ reaction” (2006).

^aAt K1.1, the number of days needed to collect data will be 2 days (full intensity) or 20 days (10% intensity).